Long-range empirical potential model: extension to hexagonal close-packed metals

2009 J. Phys.: Condens. Matter 21 385402

(http://iopscience.iop.org/0953-8984/21/38/385402)

J. Phys.: Condens. Matter **21** (2009) 385402 (10pp) doi:10.1088/0953-8984/21/38/385402

Long-range empirical potential model: extension to hexagonal close-packed metals

Y Dai, J H Li and B X Liu[1]

Advanced Materials Laboratory, Department of Materials Science and Engineering, Tsinghua University, Beijing 100084, People's Republic of China

E-mail: dmslbx@mail.tsinghua.edu.cn

Received 26 April 2009, in final form 22 June 2009
Published 24 August 2009
Online at stacks.iop.org/JPhysCM/21/385402

Abstract

An n-body potential is developed and satisfactorily applied to hcp metals, Co, Hf, Mg, Re, Ti, and Zr, in the form of long-range empirical potential. The potential can well reproduce the lattice constants, c/a ratios, cohesive energies, and the bulk modulus for their stable structures (hcp) and metastable structures (bcc or fcc). Meanwhile, the potential can correctly predict the order of structural stability and distinguish the energy differences between their stable hcp structure and other structures. The energies and forces derived by the potential can smoothly go to zero at cutoff radius, thus completely avoiding the unphysical behaviors in the simulations. The developed potential is applied to study the vacancy, surface fault, stacking fault and self-interstitial atom in the hcp metals. The calculated formation energies of vacancy and divacancy and activation energies of self-diffusion by vacancies are in good agreement with the values in experiments and in other works. The calculated surface energies and stacking fault energies are also consistent with the experimental data and those obtained in other theoretical works. The calculated formation energies generally agree with the results in other works, although the stable configurations of self-interstitial atoms predicted in this work somewhat contrast with those predicted by other methods. The proposed potential is shown to be relevant for describing the interaction of bcc, fcc and hcp metal systems, bringing great convenience for researchers in constructing potentials for metal systems constituted by any combination of bcc, fcc and hcp metals.

1. Introduction

In the past decades, a variety of empirical n-body potentials have been developed by researchers. They have attained considerable success in the study of bulk, surface, and cluster properties of metals. Examples include the embedded atom method (EAM) developed by Daw and Baskes [1, 2], the n-body potential developed by Finnis and Sinclair (FS) [3] for bcc transition metals, and the so-called TB-SMA potential developed by Tomanek *et al* [4] for fcc metals. Later, other researchers, such as Oh, Johnson, Doyama, and Zhang, proposed several short-range potentials [5–8]. These potentials commonly truncate the energies and forces with a short-range cutoff radius of less than third-nearest neighbor. In calculations of the energies and forces, the interaction of atoms is neglected if their distance is larger than the cutoff radius to save computer time in large-scale simulations. Nevertheless, an unavoidable structural stability problem is frequently encountered because they always predict the same energy for the fcc and ideal hcp structures [6]. This means that the potentials cannot correctly predict the order of structural stability. Furthermore, as most hcp metals have a particular non-ideal c/a ratio, the application of these potentials in hcp metals may bring some difficulties in predicting the right c/a ratios. In order to overcome these problems, new models for hcp metals have been developed. For example, Baskes *et al* [9] proposed modified EAM (MEAM) models, considering the angular contributions. Pasianot *et al* [10] added a new term $M(P)$ in the form of total energy for the EAM to express a many-body shear term related to bond angles in an average sense. Hu *et al* [11] developed an analytic modified embedded atom

[1] Author to whom any correspondence should be addressed.

potential (AMEAM) model by a similar approach. Chen *et al* [12] used two sets of parameters in their potential model of pure hcp metals.

These models do resolve the structural stability problem and improve some calculated properties of transition metals. Nevertheless, they also bring some application problems at the same time. For example, it is difficult to apply the models to disordered systems, such as liquid and amorphous systems, for it is difficult to define the c-axis and to calculate the angular contributions in these systems. In some works, such as in the study of the melting process, the study of crystal–amorphous state transitions and empirical potentials which can be well applied in both crystalline and disordered systems are needed. It is thus necessary to construct n-body potentials for hcp metals which can reflect their anisotropic properties and do not have terms dependent on crystalline orientation. In order to interpret the non-ideal c/a and differentiate the energy of hcp and fcc structures, adopting a longer cutoff radius greater than the third nearest-neighbor distance is an effective method for a spherically symmetric n-body potential, as the atomic configuration of the third neighbor atoms is different in fcc and ideal hcp structures.

Recently, Dai *et al* [13–15] proposed the long-range empirical potential (LREP) method with a cutoff distance larger than the fourth neighbor distance. The potential may thus distinguish the energy difference between stable and hypothetical metal structures. The long-range empirical potential (LREP) has been well applied to bcc and fcc metal systems as well as binary and ternary fcc metal systems [13–15]. It is of interest to find out whether it is possible to develop potentials for hcp metals using the LREP method. If this potential can describe the atomic interactions of hcp metals it would be more convenient for constructing empirical potentials for binary and ternary metal systems which consist of cubic and hcp metals.

In the present study, we attempt to extend the LREP so that it can be applied to hcp metals. The potential is constructed to reproduce the lattice constants and the observed c/a ratio for each hcp metal and to distinguish the energy difference between its hcp structure and other structures, such as fcc, bcc, and simple cubic (sc) structures. To evaluate the applicability of the potential, other properties, such as the cohesive energies, elastic constants, etc are also calculated and compared with experimental observations and first-principles calculation. The properties of the vacancies, divacancies, and self-interstitial atoms are studied and discussed. In addition, stacking fault energies, surface energies and some thermal properties have also been calculated and their values are compared with typical experimental data.

2. Construction of the potential

In this work, the n-body potential is constructed in the form of a LREP. According to the LREP [13–15] method, the total potential energy E_i of atom i can be calculated by

$$E_i = \tfrac{1}{2}\sum V(r_{ij}) - \sqrt{\sum \phi(r_{ij})}, \tag{1}$$

where $V(r_{ij})$ is the pair term and $\phi(r_{ij})$ is the many body part. They can be expressed as

$$V(r_{ij}) = (r_{c1} - r_{ij})^m (c_0 + c_1 r_{ij} + c_2 r_{ij}^2 + c_3 r_{ij}^3 + c_4 r_{ij}^4), \quad 0 < r_{ij} \leqslant r_{c1}, \tag{2}$$

and

$$\phi(r_{ij}) = \alpha (r_{c2} - r_{ij})^n \exp\left[-\beta\left(\frac{r_{ij}}{r_0} - 1\right)\right], \quad 0 < r_{ij} \leqslant r_{c2}. \tag{3}$$

Here, r_{c1} and r_{c2} are cutoff radii for the pair term and the many body part, respectively. r_0 is the atomic distance between the nearest-neighbor atoms in the ground state. The exponents m and n are two integers and are adjustable according to the specific metals. α, β and c_i are potential parameters that will be fitted. In the fitting process, it is found that the fitted value of parameter β is near zero. In order to simplify the form of the potential and to save computer time, the parameter β is set to be zero for the hcp metals in the present study. Thus the many body part of the potential can be written as

$$\phi(r_{ij}) = \alpha_1 (r_{c2} - r_{ij})^n, \qquad 0 < r_{ij} \leqslant r_{c2}. \tag{4}$$

As the cutoff distances are longer than the third and fourth nearest-neighbor distance, it may cost more computer time in MD simulations. However, it can be seen that the form of the pair term and the many body part are polynomial in this work. Consequently, the computation of the present developed potential is more efficient than the original LREP with an exponential term [13–15]. Generally, the potential parameters for metal systems are determined by fitting their lattice constants, cohesive energies, and elastic constants obtained in experiments. In the fitting process, these properties are calculated by the potential with a set of initial parameters first and then these parameters are adjusted by computer programs to make the calculation results closer to the experimental data or the first-principles calculation results. When a metal is in an equilibrium state, its first derivative of potential energy ($\mathrm{d}E$) should be equal to zero. Moreover, as the hcp structures do not have cubic symmetry, it should be noticed that all the elements σ_{ij} ($i, j = 1, 2, 3$) in the stress matrix σ of each unit cell should be equal to zero in the equilibrium state. Here, $\mathrm{d}E = 0$ and $\sigma_{ij} = 0$ are regarded as two fitting conditions in the present study so as to confirm the equilibrium state of a structure. After the fitting, another computation program based on the potential is applied to search the lowest energy and in a large range of lattice constants for each structure and the calculation results are consistent with the results in the fitting process. Table 1 presents the fitted potential parameters for the six hcp metals, i.e. Co, Hf, Mg, Re, Ti, and Zr.

In order to evaluate the relevance of the developed potential, the lattice constants, cohesive energies, bulk moduli, and elastic constants of the six hcp metals and those of their hypothetical bcc and fcc structures are calculated and shown in tables 2–4, with the experimental data and the results of first-principles calculations. The first-principles calculations are carried out within the context of the density functional theory using the PW91 [16, 17] generalized gradient approximation as the exchange–correlation functional and the projected

Table 1. Fitted potential parameters for Co, Hf, Mg, Re, Ti, and Zr.

	Co	Hf	Mg	Re	Ti	Zr
m	4	4	4	4	4	4
n	4	4	4	4	4	4
r_{c1} (Å)	5.00903834	6.24961864	6.54067823	5.42974107	5.81117655	6.43754936
r_{c2} (Å)	6.65369986	7.28803678	7.24230262	7.34562198	7.28149146	7.22278651
c_0 (10^{-19} J)	3.35239020	2.50996629	0.52369341	6.46677772	2.42569226	1.26299765
c_1 (10^{-19} J/Å^{m+1})	−4.50152401	−2.75569128	−0.55925561	−7.89864454	−2.87502933	−1.35558156
c_2 (10^{-19} J/Å^{m+2})	2.25585528	1.13133595	0.22344189	3.59139963	1.27417577	0.54715759
c_3 (10^{-19} J/Å^{m+3})	−0.49773155	−0.20479284	−0.03953801	−0.71825707	−0.24912625	−0.09788934
c_4 (10^{-19} J/Å^{m+4})	0.04069319	0.01374018	0.00260588	0.05330095	0.01807024	0.00653836
α_1 (10^{-19} J/Å^{n})	0.01828688	0.04833535	0.00140330	0.04538689	0.01904463	0.05782882

Table 2. The lattice constants (a), cohesive energies (E_c), bulk modulus (B_0), and elastic constants (C_{ij}) of Co, Hf, Mg, Re, Ti, and Zr obtained from LREP (first rows) and experiments [22–24] (second rows).

	Co	Hf	Mg	Re	Ti	Zr
a (Å)	2.51	3.19	3.21	2.76	2.95	3.23
	2.51	3.19	3.21	2.76	2.95	3.23
c (Å)	4.07	5.05	5.21	4.46	4.68	5.15
	4.07	5.05	5.21	4.46	4.68	5.15
E_c (eV)	4.39	6.44	1.51	8.03	4.85	6.25
	4.39	6.44	1.51	8.03	4.85	6.25
C_{11} (MBar)	2.813	1.387	0.484	5.747	1.312	1.214
	3.071	1.881	0.595	6.182	1.624	1.434
C_{12} (MBar)	1.149	0.650	0.191	2.223	0.593	0.595
	1.650	0.772	0.261	2.753	0.920	0.728
C_{13} (MBar)	1.288	1.017	0.250	2.428	0.940	0.784
	1.027	0.660	0.218	2.078	0.690	0.653
C_{33} (MBar)	4.100	2.757	0.955	7.606	2.700	2.193
	3.581	1.969	0.616	6.835	1.807	1.648
C_{44} (MBar)	0.970	0.734	0.205	1.965	0.705	0.499
	0.755	0.557	0.164	1.606	0.467	0.320
B_0 (MBar)	1.909	1.211	0.367	3.695	1.141	0.994
	1.903	1.102	0.356	3.669	1.073	0.954

Table 3. The lattice constants (a), cohesive energies (E_c), bulk modulus (B_0), and elastic constants (C_{ij}) of Co, Hf, Mg, Re, Ti, and Zr in their hypothetical bcc structure obtained from LREP (first rows) and first-principles calculations (second rows).

	Co	Hf	Mg	Re	Ti	Zr
a (Å)	2.836	3.581	3.639	3.111	3.311	3.615
	2.809	3.540	3.580	3.117	3.248	3.570
E_c (eV)	4.285	6.307	1.480	7.734	4.756	6.188
	4.284	6.266	1.478	7.715	4.744	6.179
C_{11} (MBar)	1.364	0.848	0.369	2.377	0.914	1.062
	1.538	0.663	0.216	3.639	0.841	1.326
C_{12} (MBar)	1.886	1.064	0.375	3.572	1.056	1.011
	2.186	1.201	0.382	3.557	1.228	0.799
C_{44} (MBar)	1.579	0.792	0.332	3.124	0.829	0.731
	1.259	0.513	0.322	1.800	0.330	0.635
B_0 (MBar)	1.712	0.992	0.373	3.174	1.009	1.028
	1.970	1.021	0.327	3.585	1.099	0.974

Table 4. The lattice constants (a), cohesive energies (E_c), bulk modulus (B_0), and elastic constants (C_{ij}) of Co, Hf, Mg, Re, Ti, and Zr in their hypothetic fcc structure obtained from LREP (first rows) and first-principles calculations (second rows).

	Co	Hf	Mg	Re	Ti	Zr
a (Å)	3.542	4.471	4.521	3.895	4.136	4.537
	3.520	4.475	4.524	3.918	4.100	4.527
E_c (eV)	4.376	6.406	1.496	8.003	4.820	6.220
	4.370	6.372	1.494	7.965	4.794	6.213
C_{11} (MBar)	2.544	1.394	0.434	5.141	1.278	1.029
	2.919	1.487	0.321	5.540	1.421	0.895
C_{12} (MBar)	1.269	0.708	0.230	2.486	0.657	0.670
	1.709	0.811	0.320	2.744	0.941	0.902
C_{44} (MBar)	0.951	0.428	0.185	2.024	0.424	0.386
	1.480	0.629	0.188	2.066	0.558	0.277
B_0 (MBar)	1.694	0.937	0.298	3.371	0.864	0.790
	2.113	1.036	0.320	3.676	1.101	0.900

augmented wave (PAW) [18, 19] method, as implemented in the Vienna *ab initio* simulation package (VASP) [20]. The integration in the Brillouin zone is done in a mesh of $11 \times 11 \times 11$ special k-points (56 irreducible k-points for bcc and fcc lattice and 96 irreducible k-points for hex lattice) determined according to the Monkhorst–Pack scheme [21], as such an integration has proved to be sufficient for the computation of these simple structures in this work. The first-principles simulations were spin-polarized for all the six metals, Co, Hf, Mg, Re, Ti, and Zr, although some of them are non-ferromagnetic metals. It can be seen that the calculated lattice constants, cohesive energies, and bulk moduli of the six metals match well with their experimental values and first-principles calculation results in their stable hcp structure and in hypothetical bcc or fcc structure. The elastic constants derived by empirical potential are generally consistent with those obtained in experiments and first-principles calculations, while their agreements are not as good as those of the other properties, such as the lattice constants and the cohesive energies. Considering the limitation of the spherical symmetric potential and the errors of the first-principles calculations or the experiments, these discrepancies can be accepted. It can also be seen that they exactly reproduce the experimental c/a ratio for each metal. This implies that the constructed potential may be correct for the anisotropic properties of hcp metals although they are spherical symmetric.

Table 5. The structural energy differences ΔE(eV/atom) obtained by the LREP, first-principles calculations, experimental observations [9], MEAM potential [9], and AMEAM potential [11].

	Methods	Co	Hf	Mg	Re	Ti	Zr
$\Delta E_{\text{hcp}\to\text{ideal hcp}}$	LREP	0.0007	0.0058	0.0003	0.0024	0.0036	0.0034
	MEAM	0.0000	0.0059	0.0000	0.0005	0.0071	0.0105
	AMEAM	0.0000	0.0068	0.0001	0.0018	0.0041	0.0029
$\Delta E_{\text{hcp}\to\text{fcc}}$	LREP	0.0148	0.0353	0.0139	0.0277	0.0299	0.0302
	Ab initio	0.0196	0.0681	0.0161	0.0652	0.0565	0.0367
	Expt.		0.100	0.026	0.110	0.060	0.076
	MEAM	0.005	0.053	0.004	0.031	0.033	0.017
	AMEAM	0.0062	0.0068	0.0022	0.0050	0.0094	0.0049
$\Delta E_{\text{hcp}\to\text{bcc}}$	LREP	0.1057	0.1337	0.0298	0.2968	0.0941	0.0631
	Ab initio	0.1064	0.1742	0.0324	0.3145	0.1057	0.0707
	Expt.		0.059	0.031	0.292	0.070	0.076
	MEAM	0.241	0.064	0.029	0.303	0.075	0.061
	AMEAM	0.0164	0.0301	0.0176	0.1636	0.0143	0.0179
$\Delta E_{\text{hcp}\to\text{diamond}}$	LREP	1.0742	1.6701	0.6381	1.8894	1.2699	1.6169
	MEAM	1.20	2.19	0.31	2.39	1.57	1.48
$\Delta E_{\text{hcp}\to\text{sc}}$	LREP	0.2652	0.1654	0.1471	0.5967	0.1631	0.3835
	MEAM	0.5900	0.5100	0.1300	0.9400	0.4100	0.4500

It is very important to ensure that no unphysical structural instabilities would occur for a potential in the calculations. Based on the newly developed LREP potential, we calculate the energies of metastable structures, i.e. ideal hcp, fcc, bcc, diamond, and sc structures, of the six hcp metals. Table 5 shows the calculated energy differences between the metastable structures (ideal hcp, fcc, bcc, diamond structures, sc) and the hcp one, i.e. $\Delta E_{\text{hcp}\to\text{ideal hcp}}$, $\Delta E_{\text{hcp}\to\text{bcc}}$, $\Delta E_{\text{hcp}\to\text{fcc}}$, $\Delta E_{\text{hcp}\to\text{diamond}}$, and $\Delta E_{\text{hcp}\to\text{sc}}$. For comparison, the results obtained from experimental observations and first-principles calculations are also listed in table 5.

One sees that the values of energy differences predicted by the present model quantitatively match with those obtained from experiments or first-principles calculations. Both the calculated results and experimental ones indicate that hcp structure has the lowest potential energy among hcp, ideal hcp, fcc, bcc, sc, and diamond structures, reflecting the fact that the equilibrium states of the six metals are all hcp structures. In table 5, inspecting the values of $\Delta E_{\text{hcp}\to\text{ideal hcp}}$ predicted by LREP and other works, the results of the constructed potential are in general agreement with other works, especially for AMEAM [11]. Meanwhile, the $\Delta E_{\text{hcp}\to\text{ideal hcp}}$ predicted by LREP for metals with a near-ideal c/a ratio ($\sqrt{8/3} \approx 1.633$), Co and Mg, are larger than those in other works. These energy differences are in a reasonable range, as the absolute values of all these results are much lower than those of other metals. Inspecting the values of $\Delta E_{\text{hcp}\to\text{fcc}}$ and $\Delta E_{\text{hcp}\to\text{bcc}}$, one sees that the results of the constructed potential and MEAM [9] are quantitatively consistent with each other, while the results of AMEAM [11] have been systematically underestimated compared to the experimental results, as the maximum relative error is beyond 90%. Apparently, the constructed potential is more relevant than AMEAM [11] in predicting the structural stability of hcp transition metals. Inspecting the values of $\Delta E_{\text{hcp}\to\text{diamond}}$ and $\Delta E_{\text{hcp}\to\text{sc}}$, one sees that the results of the constructed potential and MEAM [9] are qualitatively consistent with each other. The agreement of $\Delta E_{\text{hcp}\to\text{diamond}}$ in this work and MEAM [9] is rather good and is better than that of $\Delta E_{\text{hcp}\to\text{sc}}$ except for Mg. The calculation results in this work and MEAM [9] are in overall agreement. These results imply that the developed potential can reasonably predict the structural stability and distinguish the energy difference between the hcp structures and other structures.

In order to check the relevance of an empirical potential, the equation of state is often derived from the potential and then compared with that obtained in other ways. The frequently used equations of state in this field are the Rose equation [25] and its variant [26], which have been considered to be universal for all categories of metals. The equations of state, i.e. the total energy as a function of the lattice constant, are calculated in the present study. The predictions of the constructed potential are compared in figure 1 with the results obtained from the Rose equation for the six metals. One sees that there is no discontinuity of the curves in the whole calculated range. In particular, at the cutoff radius, the potential energy and its derivative continuously go to zero as expected for each metal. It can also be seen that the total energy derived from the proposed potential is close to the Rose equation in the vicinity of the equilibrium point, indicating that the interatomic potential developed in the present study can be applied to describe the interatomic interaction of a system if it is not far from the equilibrium state.

In the following sections, the developed potential is applied to study some basic scientific issues, such as the vacancies, divacancies, self-interstitial atoms, stacking faults, and surfaces. These issues themselves are of significance and hence worth further studies in order to reveal their underlying physics as well as their respective atomic mechanisms. Meanwhile, if the calculation results are in agreement with the experimental observations and other theoretical predictions, they could serve as further evidence confirming the relevance of the developed potentials.

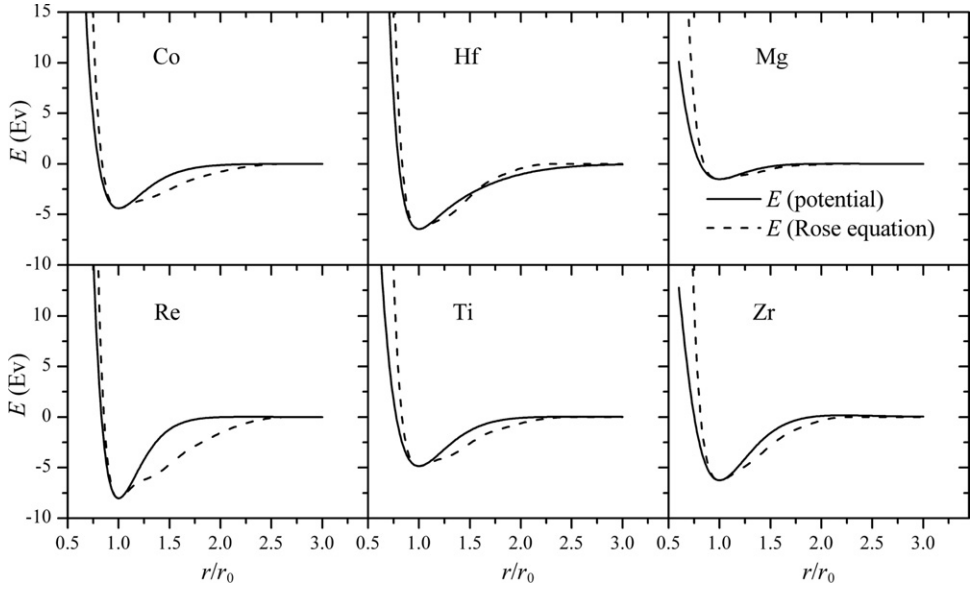

Figure 1. Total energies E as a function of lattice constant calculated from the LREP and Rose equation.

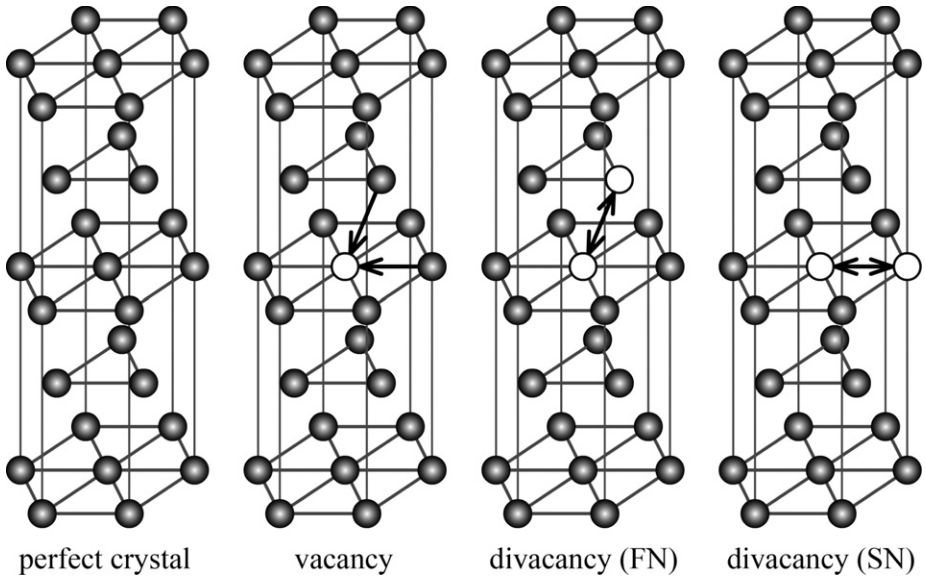

Figure 2. The schematic representations of the vacancy and divacancy configurations in the hcp structure. The open circles stand for vacancies.

3. Vacancies and divacancies

Based on the developed potential, the vacancy formation energies (E_{1v}), the vacancy migration energies (E_{1m}), the activation energies for self-diffusion by the vacancy mechanism (Q_{1v}), and the divacancy formation energies (E_{2v}) are calculated by molecular dynamics (MD) simulations and presented in table 6. Schematic representations of the vacancy and divacancy configurations in hcp structure are presented in figure 2. The MD simulations are carried out with the Parrinello–Rahman constant pressure scheme [27] at 3 K and 0 Pa. The equations of motion are solved using the second-order four-value predictor corrector algorithm of Gear with a time step of 5×10^{-15} s [28]. In the models, the $[2\bar{1}\bar{1}0]$, $[0\bar{1}10]$, and [0001] crystalline directions are parallel to the x, y, and z axes, respectively. Periodic boundary conditions are adopted in the three axes. In the calculations, the models consist of $10 \times 12 \times 6 = 720$ unit cells (1440 atoms for perfect crystal, 1439 atoms for monovacancy and 1438 atoms for divacancy). In the calculation of the migration energy for a vacancy, one atom is pushed towards the nearest vacant site by changing its velocity artificially. The movement of the atom is monitored by its position and energy. The vacancy migration energy is the energy corresponding to the lowest velocity for the atom moving from its crystal site to the vacant site. For hcp metals, there are two favorable paths for the migration of a vacancy, corresponding to the migration of an atom out of the basal plane and in the basal plane, the migration energy of which are denoted as E_{1m}^{out} and E_{1m}^{in} respectively. The self-diffusion activation energy by the vacancy mechanism is sum of the

Table 6. Vacancy migration energy and self-diffusion activation energy by the vacancy mechanism (eV) obtained by the LREP, experimental observations, and other works.

Metals	Value	Calculated	Expt.	Data in other works
Co	E_{1v}	1.40	1.35 [9]	1.48 [9], 1.38 [11], 1.41 [29]
	E_{1m}^{out}	0.93		0.72 [11], 0.89 [29]
	Q_{1v}^{out}	2.33		2.10 [11], 2.301 [29]
	E_{1m}^{in}	0.87		0.72 [11], 0.89 [29]
	Q_{1v}^{in}	2.27		2.10 [11], 2.30 [29]
Hf	E_{1v}	1.98	1.80 [9]	2.02 [9], 1.80 [11]
	E_{1m}^{out}	0.63		0.90 [11]
	Q_{1v}^{out}	2.61		2.70 [11]
	E_{1m}^{in}	0.75		0.98 [11]
	Q_{1v}^{in}	2.73		2.78 [11]
Mg	E_{1v}	0.79	0.58 [9], 0.87 [30]	0.66 [9], 0.59 [11], 0.87 [31]
	E_{1m}^{out}	0.43	0.39 [31]	0.35 [11], 0.66 [30]
	Q_{1v}^{out}	1.22	1.388 [32]	0.94 [11], 1.26 [31], 1.43 [33, 38]
	E_{1m}^{in}	0.40		0.35 [11], 0.59 [30], 0.40 [31]
	Q_{1v}^{in}	1.19		0.94 [11], 1.38 [30], 1.27 [31], 1.44 [33]
Re	E_{1v}	2.30	2.30 [9]	2.49 [9], 2.35 [11]
	E_{1m}^{out}	2.54		2.25 [11]
	Q_{1v}^{out}	4.84		4.60 [11]
	E_{1m}^{in}	2.39		2.29 [11]
	Q_{1v}^{in}	4.69		4.64 [11]
Ti	E_{1v}	1.59	1.50 [9]	1.80 [9], 1.49 [11, 34, 36], 1.43 [35]
	E_{1m}^{out}	0.52		0.56 [11], 0.82 [34], 1.28 [36], 0.68 [37]
	Q_{1v}^{out}	2.11	1.272 [47]	2.05 [11], 2.31 [34], 2.77 [36], 3.014 [38]
	E_{1m}^{in}	0.58		0.61 [11], 0.67 [34], 1.28 [36], 0.80 [37]
	Q_{1v}^{in}	2.17		2.10 [11], 2.16 [34], 2.77 [36]
Zr	E_{1v}	1.75	1.70 [9]	1.93 [9], 1.70 [11], 1.55 [39],1.86 [40]
	E_{1m}^{out}	0.92		0.67 [11], 0.785 [40], 1.07 [39]
	Q_{1v}^{out}	2.67		2.37 [11], 2.645 [40], 2.62 [39]
	E_{1m}^{in}	0.89		0.72 [11], 0.775 [40], 1.18 [39]
	Q_{1v}^{in}	2.64		2.42 [11], 2.635 [40], 2.73 [39], 3.296 [38]

vacancy formation energy and the vacancy migration energy, which can be calculated by

$$Q_{1v}^{out} = E_{1m}^{out} + E_{1v} \tag{5}$$

$$Q_{1v}^{in} = E_{1m}^{in} + E_{1v}. \tag{6}$$

The calculated results and experimental data are listed in table 6. The present calculation results of the formation energies and diffusion activation energies of vacancies are agree well with the experimental data. These results are also in general agreement with other calculation results.

It is of interest to compare the out-of-basal plane and in-basal plane self-diffusion energy, since the available data are limited and contradictory [11]. The present study reveals that Q_{1v}^{out} is larger than Q_{1v}^{in} for Co, Mg, Re, and Zr, so diffusion in the basal plane is easier than in the non-basal plane for these metals. Meanwhile, for Hf and Ti, Q_{1v}^{out} is less than the Q_{1v}^{in}, so diffusion in the non-basal plane is easier than that in the basal plane for these metals. Our calculations implied that the micro-diffusion mechanism is strongly affected by the c/a ratio, as the c/a ratios of Hf and Ti have the smallest values, which are less than 1.59, while those of the others are all larger than 1.59.

The application of the developed potential to the divacancy properties can further evaluate the reliability of the potential. We therefore investigate the divacancy formation and binding energies for two divacancy configurations, first-nearest neighbors (in different basal planes) and second-nearest neighbors (in the same basal plane), which are much more stable than other configurations. The divacancy binding energy is the difference between the energies of two well-separated vacancies and two neighbor vacancies. The calculated results are presented in table 7 along with the calculation results from other works. It can also be seen that the formation energies for different configurations are almost the same in each work, although the divacancy formation energies obtained in different works are somewhat different in magnitude. From table 7, one can find that all the binding energies are positive in this

Table 7. Divacancy formation and binding energies (eV) obtained by the LREP and other works.

	Divacancy in plane		Divacancy out of plane	
Metal	E_{2v}^{in}	E_{2v}^{in}	E_{2v}^{out}	$E_{2v}^{b\ out}$
Co	2.71	0.08	2.72	0.08
		−0.47 [9]		−0.46 [9]
		0.440 [29]		0.40 [29]
	2.57 [11]	0.19 [11]	2.56 [11]	0.2 [11]
Hf	3.76	0.20	3.78	0.18
		−0.21 [9]		−0.18 [9]
	3.35 [11]	0.24 [11]	3.35 [11]	0.24 [11]
Mg	1.47	0.11	1.48	0.11
		−0.22 [9]		−0.22 [9]
		0.133 [41]		0.131 [41]
	1.09 [11]	0.09 [11]	1.1 [11]	0.08 [11]
Re	4.48	0.13	4.49	0.12
		−0.63 [9]		−0.61 [9]
	4.4 [11]	0.32 [11]	4.38 [11]	0.32 [11]
Ti	3.03	0.16	3.04	0.14
		−0.13 [9]		−0.11 [9]
	2.76 [34]	0.22 [34]	2.76 [34]	0.22 [34]
	2.36 [42]	0.62 [36]	2.58 [42]	0.40 [36]
	2.79 [11]	0.20 [11]	2.76 [11]	0.22 [11]
Zr	3.30	0.20	3.31	0.19
		−0.53 [9]		−0.52 [9]
		0.248 [40]		0.236 [40]
		0.10 [43]		0.08 [43]
	3.18 [11]	0.22 [11]	3.18 [11]	0.21 [11]

work. This means that all these configurations are stable as predicted by the constructed potential. In other works, the binding energies are all positive except for the results obtained by MEAM [9].

4. Self-interstitial atoms

In this work, MD simulations are applied to calculate the properties of self-interstitial atoms for eight different configurations suggested by Johnson *et al* [36]. According to their suggestion, the O site has an octahedral coordination; the T site has a tetrahedron coordination; the S site represents a [0001] split dumbbell, i.e., two atoms sharing the same site in the *c* direction; and the C site is midway between two nearest-neighbor atoms out of the basal plane, and can be viewed as a pseudo-crowdion. The other four configurations are in the basal plane: the BO site is below an O site; the BT site is below a T site, the BC site is midway between two nearest neighbors in the basal plane; and the BS site involves two atoms equidistant from a vacant lattice site. The schematic representations of these configurations in the hcp structure investigated in the present study are presented in figure 3.

In the MD simulations, unstable configurations are relaxed and transform to a stable (or metastable) one. The relaxed configuration for each initial site and the formation energy for stable (or metastable) configurations are presented in table 8. The non-basal dumbbell is denoted as DB in the table. It can be seen that O and BS are stable for all the six hcp metals. In the MD simulations, BC, BO, BS, and BT would transform to

Table 8. The final state and formation energies for self-interstitial atoms (eV) at different positions derived from LREP.

	Final state					
Initial state	Co	Hf	Mg	Re	Ti	Zr
O	O	O	O	O	O	O
E_{SIA_O}	4.97	4.78	1.96	13.25	3.77	4.16
BC	BS	BS	BS	BS	BS	BS
BO	BS	BS	BS	BS	BS	O
BS	BS	BS	BS	BS	BS	BS
E_{SIA_BS}	4.34	3.93	1.77	12.03	3.12	3.21
BT	BS	BS	BS	BS	BS	BS
C	DB	O	O	DB	O	O
T	BS	BS	BS	BS	O	O
S	DB	O	O	DB	O	O
E_{SIA_DB}	4.32			11.88		

BS for the six metals, except that BO would transform to O for Zr. C and S transform to DB (Co and Re), and O (Hf, Mg, Ti, and Zr). T would transform to BS (Co, Hf, Mg, and Re) and O (Ti, and Zr). From the calculated formation energy of the self-interstitial atom, it can be found that BS is the most stable configuration for Hf, Mg, Ti, and Zr, while DB is the most stable configuration for Co and Re. However, different stable configurations of self-interstitial atoms are derived by different potentials. For instance, Hu *et al* [11] reported that the most stable self-interstitial atom is BS for Be and Ru, BS or BC for Hf, Sc, Y, and Zr, and is non-basal dumbbell for Co, Mg, Re, and Ti. Igarashi *et al* [45] reported that the pyramidal plane crowdion is most stable for Co, Mg, Hf, Ti, and Zr. Bacon [37] reported that the basal octahedral site is most stable with pair potential calculations for Co, Ti, and Zr. These calculation results somewhat contrast with the present work. As stable states derived by different potentials are different, it is inconvenient to list the calculated formation energies derived by others in the same table. Comparing the formation energies calculated in this work and in other works, the calculated results in the present work are in general agreement with the results in other works [5, 11, 44, 46–50] in magnitude, although the predicted results are much smaller than those obtained by Igarashi *et al* [45].

5. Surface and stacking fault energy

The developed potential is applied to calculate the surface energy of low index faces, the basal plane (0001), and the prism plane $(0\bar{1}10)$ through MD simulations. The calculated models consist of $10 \times 12 \times 12 = 1440$ unit cells (2880 atoms) for the surface energies in the basal plane and $20 \times 12 \times 12 = 1440$ unit cells (2880 atoms) for those in the prism plane. The difference in the surface energy between relaxed and unrelaxed values for the basal plane or the prism plane is small, no more than 5 mJ m^{-2}. The calculated surface energies are presented in table 9. The calculated surface energy of the basal plane for each metal is a bit lower than that of the prism plane, as the surface atom density of the basal plane is higher than that of the prism plane for the six hcp metals with the c/a ratio below the ideal value. The surface energies derived by the constructed potential are lower than the experimental data and the results

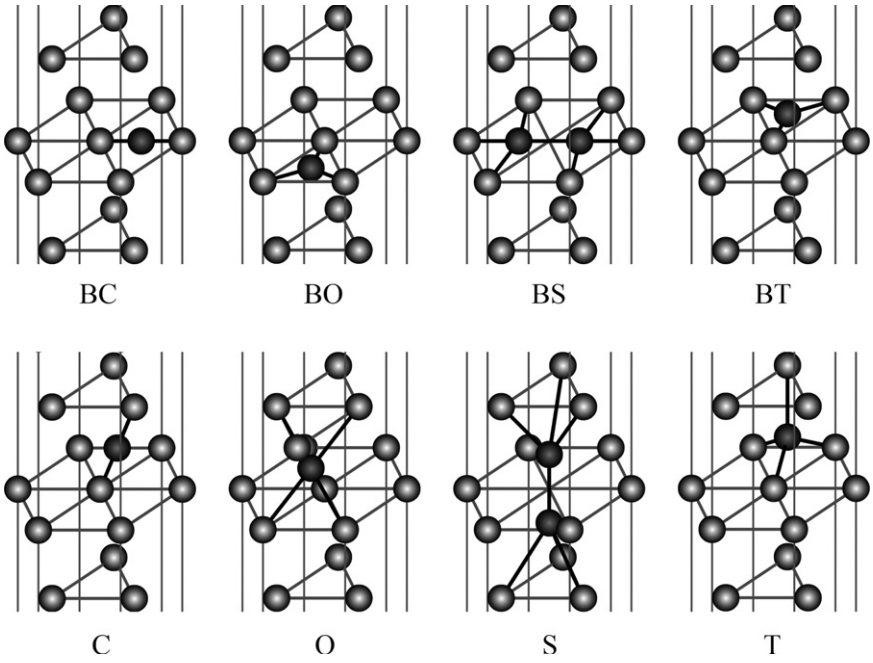

Figure 3. The schematic representations of the self-interstitial configurations in the hcp structure. The black balls represent self-interstitial atoms.

Table 9. Stacking fault energies (mJ m^{-2}) obtained by the LREP, experimental observations [51], and other works.

	Co	Hf	Mg	Re	Ti	Zr
I1	44	68	25	70	68	56
	18 [11]	22 [11]	12 [11]	44 [11]	71 [11]	40 [11]
					33 [35]	41 [44]
I2	66	101	38	104	101	84
	30 [9]	198 [9]	14 [9]	150 [9]	144 [9]	62 [9]
	37 [11]	45 [11]	8 [11]	31 [11]	47 [11]	26 [11]
					64 [35]	80 [44]
	64 [45]	111 [45]	10 [45]		116 [45]	27 [45]
	42 [51]	390 [51]	30 [51]	540 [51]	290 [51]	340 [51]
E	131	200	76	206	200	166
	55 [11]	67 [11]	12 [11]	44 [11]	71 [11]	40 [11]
					94 [35]	118 [44]

of MEAM [9], and higher than the results of AMEAM [11]. It can be seen that the calculated surface energy of Co matches well with the experimental value, and other calculation results are comparable to those data obtained from experiment or other theoretical works.

The energies of a few stacking faults, such as two intrinsic faults I1 (ABABCBCB stacking sequence) and I2 (ABABCACA stacking sequence) and the extrinsic fault E (ABABCABAB stacking sequence), were calculated based on the constructed potential as well. These calculations were carried out by MD simulations with models containing some 2880 atoms. The calculated stacking fault energies are presented in table 10. As fault I2 can be formed from the perfect crystal by a simple shear, most calculation results are reported concerning this stacking. Considering that stacking fault energies are not at all well known, it can be seen that reasonable stacking fault energies of I2 are predicted by the constructed potential for the six metals. In table 10, it can be seen that the fault energy for I1 is about half of that of I2 and that of fault E is about 1.5 times that of I2 in the present calculations, which has been pointed out by Baskes *et al* [9] for MEAM and pair potentials. From the results, it can be seen that the developed potential can reasonably reflect the behavior of stacking faults in hcp metals.

As one can see, the proposed potential can correctly predict the order of structural stability and distinguish the energy differences between their stable structure and other structures. It can also well predict the behaviors of vacancies, self-interstitial atoms, and some other defects in hcp metals. However, since it is based on a semi-empirical method, there are still some properties that cannot be well derived from the proposed potential. For example, the melting points and linear thermal expansion coefficients (300 K) are calculated through MD simulations and shown in figure 4. The corresponding experimental values [22, 53] are also presented for comparison in the figure. One notes that the calculated melting points are somehow lower than the experimental values and the calculated expansion coefficients for most elements are much

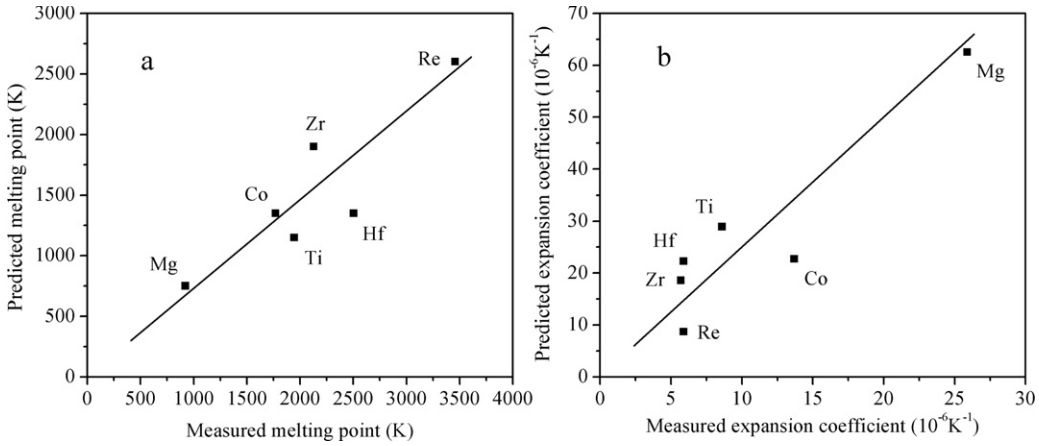

Figure 4. The melting points (a) and linear thermal expansion coefficients (b) of Co, Hf, Mg, Re, Ti, and Zr derived from the proposed n-body potential through MD simulation.

Table 10. Surface energy (mJ m^{-2}) obtained by the LREP, experimental observations [52], and other works.

	Co	Hf	Mg	Re	Ti	Zr
Basal plane	1893	1463	437	2625	1442	1097
	3056 [9]	2041 [9]	900 [9]	3940 [9]	1962 [9]	1001 [9]
	1162 [11]	992 [11]	310 [11]	1682 [11]	1033 [11]	623 [11]
Prism plane	1943	1534	451	2695	1498	1156
	3459 [9]	1636 [9]	1016 [9]	3949 [9]	1673 [9]	2364 [9]
	1172 [11]	988 [11]	316 [11]	1689 [11]	1023 [11]	978 [11]
	2160 [52]	2190 [52]	785 [52]	3630 [52]	1920 [52]	2050 [52]

higher than the experimental data. Although the developed potential cannot reproduce these thermal properties, the developed potential can well predict the properties related to the energy and phase stability of hcp metals.

6. Concluding remarks

A spherically symmetric potential has been developed and satisfactorily applied to six hcp metals, Co, Hf, Mg, Re, Ti, and Zr. The developed potential can well reproduce the lattice constants, c/a ratios, cohesive energies, and bulk moduli for the stable hcp structure and metastable bcc and fcc structures. Meanwhile, the energy differences between the real hcp structure and ideal hcp, fcc, bcc, sc, and diamond structures are calculated. These calculations show that the developed potential can correctly predict the order of structural stability and reasonably distinguish the energy differences between their stable hcp structure and other structures.

Based on the developed potential, the properties of the defects in the hcp metals are studied as well. The calculated vacancy formation energies, the activation energies of self-diffusion by vacancies and the divacancy formation energies are in good agreement with the values in experiments and in other works. Although the stable configurations of self-interstitial atoms predicted in this work somewhat contrast with those predicted by other methods, the calculated formation energies generally agree with the values in other works. The calculated surface energies and stacking fault energies are also consistent with the experimental results or theoretical predictions.

As the developed potential is spherically symmetric, it may be applied in general calculations or large-scale simulations including their ordered and disordered states. Meanwhile, since the potential is in an analytic form which has been well applied to bcc and fcc metals, it is more convenient to construct empirical potentials for a metal system which consists of cubic and hcp metals.

Acknowledgment

The authors are grateful for financial support from the National Natural Science Foundation of China (50531040 and 50871058), the Ministry of Science and Technology of China (2006CB605201), and the Administration of Tsinghua University.

References

[1] Daw M S and Baskes M I 1983 *Phys. Rev. Lett.* **50** 1285
[2] Daw M S and Baskes M I 1984 *Phys. Rev.* B **29** 6443
[3] Finnis M W and Sinclair J E 1984 *Phil. Mag.* A **50** 45
[4] Tomanek D, Aligia A A and Balseiro C A 1985 *Phys. Rev.* B **32** 5051
[5] Oh D J and Johnson R A 1988 *J. Mater. Res.* **3** 471
[6] Johnson R A and Oh D J 1989 *J. Mater. Res.* **4** 1195
[7] Doyama M and Kogure Y 1999 *Comput. Mater. Sci.* **14** 80
[8] Zhang B W, Ouyang Y F, Liao S Z and Jin Z P 1999 *Physica* B **262** 218
[9] Baskes M I and Johnson R A 1994 *Modelling Simul. Mater. Sci. Eng.* **2** 147

[10] Pasianot R, Farkas D and Savino E J 1991 *Phys. Rev.* B **43** 6952
[11] Hu W, Zhang B, Gao F and Bacon D 2001 *J. Phys.: Condens. Matter* **13** 1193
[12] Chen S, Xu J and Zhang H 2004 *Comput. Mater. Sci.* **29** 428
[13] Dai X D, Kong Y and Li J H 2007 *Phys. Rev.* B **75** 104101
[14] Dai X D, Li J H and Kong Y 2007 *Phys. Rev.* B **75** 052102
[15] Dai X D, Li J H and Liu B X 2007 *Appl. Phys. Lett.* **90** 131904
[16] Perdew J P and Wang Y 1992 *Phys. Rev.* B **45** 13244
[17] Perdew J P, Chevary J A, Vosko S H, Jackson K A, Pederson M R, Singh D J and Fiolhais C 1992 *Phys. Rev.* B **46** 6671
[18] Blochl P E 1994 *Phys. Rev.* B **50** 17953
[19] Kresse G and Joubert D 1999 *Phys. Rev.* B **59** 1758
[20] Kresse G 2003 Vienna ab initio simulation package (VASP) http://cms.mpi.univie.ac.at/vasp/vasp/vasp.html
[21] Monkhorst H J and Pack J D 1976 *Phys. Rev.* B **13** 5188
[22] Kittel C 1996 *Introduction to Solid State Physics* (New York: Wiley)
[23] Simmons G and Wang H 1971 *Single Crystal Elastic Constants and Calculated Aggregate Properties: a Handbook* 2nd edn (Cambridge: MIT Press)
[24] Lide D R 2002 *CRC Handbook of Chemistry and Physics* (New York: CRC Press)
[25] Guinea F, Rose J H, Smith J R and Ferrante J 1984 *Appl. Phys. Lett.* **44** 53
[26] Li J H, Liang S H, Guo H B and Liu B X 2005 *Appl. Phys. Lett.* **87** 194111
[27] Parrinello M and Rahman A 1981 *J. Appl. Phys.* **52** 7182
[28] Allen M P and Tildesley D J 1987 *Computer Simulation of Liquids* (London: Oxford University Press)
[29] Beeler J R and Beeler M F 1981 *Interatomic Potentials and Crystalline Defects* (New York: The Metallurgical Society AIME)
[30] Bisio P H and Monti A M 1986 *Phys. Status Solidi* b **135** 545
[31] Liu X, Adams J B, Ercolessi F and Moriarty J A 1996 *Modelling Simul. Mater. Sci. Eng.* **4** 293
[32] Shewmon P G and Rhines F N 1954 *Trans. TMS-AIME* **200** 1021
[33] Combronde J and Brebec G 1971 *Acta Metall.* **19** 1393
[34] Johnson R A 1991 *Phil. Mag.* A **63** 865
[35] Ackland G J 1992 *Phil. Mag.* A **66** 917
[36] Johnson R A and Beeler J R 1981 *Interatomic Potentials and Crystalline Defects* (New York: The Metallurgical Society AIME) p 165
[37] Bacon D J 1993 *J. Nucl. Mater.* **249** 206
[38] Cahoon J R and Sherby O D 1992 *Metall. Trans.* A **23** 2491
[39] Fuse M J 1985 *Nucl. Mater.* **136** 250
[40] Oh D J and Johnson R A 1989 *J. Nucl. Mater.* **169** 5
[41] Bacon D J 1988 *J. Nucl. Mater.* **159** 176
[42] Adda Y and Philibert J 1966 *La Diffusion Dans les Solides* vol II (Paris: Presses Universitaires De France) p 1132
[43] Mikhin A G, Osetsky Y N and Kapinos V G 1994 *Phil. Mag.* A **70** 25
[44] Ackland G J, Wooding S J and Bacon D J 1995 *Phil. Mag.* A **71** 553
[45] Igarashi M, Khantha K and Vitek V 1991 *Phil. Mag.* B **63** 603
[46] Jelinek B, Houze J, Kim S, Horstemeyer M F, Baskes M I and Kim S G 2007 *Phys. Rev.* B **75** 054106
[47] Wen M, Woo C H and Huang H C 2000 *J. Comput. Aided Mol. Des.* **7** 243
[48] Johnson R A 1991 *Phil. Mag.* A **63** 865
[49] Willaime F 2003 *J. Nucl. Mater.* **323** 205
[50] Mikhin A G, Osetsky Y N and Kapinos V G 1994 *Phil. Mag.* A **70** 25
[51] Legrand P B 1984 *Phil. Mag.* B **49** 171
[52] Tyson W R and Miller W A 1977 *Surf. Sci.* **62** 267
[53] Kirby R, Hahn T and Rothrock B 1972 *American Institute of Physics Handbook* (New York: McGraw-Hill)